Toxicology 526 (2026) 154533

Contents lists available at ScienceDirect

Toxicology

journal homepage: www.elsevier.com/locate/toxicol

Polystyrene nanoplastics impair epithelial barrier establishment and modulate extracellular vesicle release in human bronchial cells cultured at the air-liquid interface

Cristina Milillo [a,b,1], Annalisa Bruno [a,b,1], Francesca D'Ascanio [a,c,d], Marco Gatta [a,b], Michela Battistelli [e], Sabrina Burattini [e], Piero Di Carlo [a,b], Jorge Parrón-Ballesteros [f], Elena Niccolai [g], Melania Dovizio [a,b,*], Paola Lanuti [a,c], Eva Batanero [f], Amedeo Amedei [g], Patrizia Ballerini [a,b]

[a] Center for Advanced Studies and Technology (CAST), "G. d'Annunzio" University of Chieti-Pescara, Chieti, Italy
[b] Department of Innovative Technologies in Medicine & Dentistry, "G. d'Annunzio" University of Chieti-Pescara, Chieti, Italy
[c] Department of Medicine and Aging Sciences, "G.d'Annunzio" University of Chieti-Pescara, Chieti, Italy
[d] Department of Humanities, Law and Economics, "Leonardo da Vinci" University, Torrevecchia Teatina 66010, Italy
[e] Department of Biomolecular Sciences, University of Urbino Carlo Bo, Urbino 61029, Italy
[f] Department of Biochemistry and Molecular Biology, Faculty of Chemistry, Complutense University of Madrid, Madrid, Spain
[g] Department of Experimental and Clinical Medicine, University of Florence, Florence, Italy

ARTICLE INFO

Keywords:
Polystyrene nanoplastics
Airway epithelium
Air-liquid interface culture
Epithelial barrier
Extracellular vesicles
Osteopontin

ABSTRACT

The growing production of plastics has led to widespread environmental contamination by micro- and nanoplastics (MNPLs), raising increasing concern about their potential impact on human respiratory health. Among them, nanoplastics (NPs) can penetrate deeply into the lungs. However, their impact on human bronchial epithelial cells remains poorly characterized. Here, we assessed the effects of 40 nm polystyrene (PS)-NPs on human bronchial Calu-3 cells cultured at the air-liquid interface (ALI) during early epithelial establishment, a three-dimensional model representing a functionally immature or compromised airway epithelial barrier. Chronic exposure (120 h) to PS-NPs (12 and 120 μg/cm^2) interfered with barrier establishment in a concentration- and time-dependent manner, as demonstrated by reduced transepithelial electrical resistance (TEER) and decreased expression of the junctional proteins E-cadherin and Zonula Occludens-1 (ZO-1). PS-NPs also promoted the release of multiple inflammatory mediators, with osteopontin (OPN), a recognized biomarker of air pollution exposure, together with IL-2 and IL-10, showing the most consistent increases across both epithelial compartments. Other cytokines displayed concentration- and compartment-dependent secretion patterns. This polarized secretion pattern suggests selective activation of epithelial signaling pathways and paracrine communication toward the submucosal milieu. Furthermore, PS-NPs were internalized by Calu-3 cells and packaged into extracellular vesicles (EVs), a process that may limit acute cellular damage while potentially enabling propagation of NP-induced signals. Overall, these findings indicate that PS-NP exposure perturbs epithelial barrier function and polarized intercellular communication under conditions mimicking a compromised airway epithelium, suggesting a mechanistic role for NPs as aggravating factors of pre-existing epithelial dysfunction.

1. Introduction

The increasing global plastic production, currently exceeding 400 million tons per year (Plastics – the fast Facts, 2024, https://plasticseurope.org/knowledge-hub/plastics-the-fast-facts–2024), is associated with a growing accumulation of environmental plastic waste. Plastics,

* Correspondence to: Department of Innovative Technologies in Medicine & Dentistry, "G. d'Annunzio" University of Chieti-Pescara, Via dei Vestini, 31, Chieti 66100, Italy.
E-mail address: m.dovizio@unich.it (M. Dovizio).
[1] These authors contributed equally

https://doi.org/10.1016/j.tox.2026.154533
Received 18 February 2026; Received in revised form 5 June 2026; Accepted 23 June 2026
Available online 25 June 2026

engineered to be resilient, do not readily degrade. When entering the environment, they undergo progressive physical and chemical fragmentation, leading to the formation of microplastics (MPs) (<5 mm) and nanoplastics (NPs) (<1 μm), collectively referred to as micro-nanoplastics (MNPLs) (Gigault et al., 2018), which are found in the air and water.

In the atmosphere, primary MNPL sources include tire abrasion, agricultural activities, textiles, and paints (Sharaf Din et al., 2024). Accurate quantification and lifetime accumulation remain challenging due to detection limits and sampling complexities, mainly for NPs in the air (Xie et al., 2022). The small size of NPs enables them to penetrate deeply into the lower airways and translocate across the bronchial and alveolar epithelial barriers (Geiser and Kreyling, 2010). Therefore, the presence of MNPLs in all regions of the respiratory system (Jenner et al., 2022) and in the bloodstream (Leslie et al., 2022) has strongly fuelled concerns about their potential risks to human health. An association between high exposure to NPs and the onset/exacerbation of respiratory diseases, such as asthma, chronic obstructive pulmonary disease (COPD), pulmonary fibrosis, and tumors, has been described (Gou et al., 2024).

Over the last decade, there has been an exponential growth in research on the complex and multifaceted nature of NP toxicity, highlighting that several factors, including size, surface charge, and polymer type, significantly contribute to the harmful effects of these particles, especially on the respiratory system (Viana et al., 2025). In this regard, in vitro studies have reported NP-induced cytotoxicity in bronchial and alveolar epithelial models, with additional findings linking these exposures to oxidative stress and pro-inflammatory responses (Shahzadi et al., 2023; Wu et al., 2024; Milillo et al., 2024; Vattanasit et al., 2023). In vivo administration of NPs, either via inhalation or intratracheal instillation, elicited a pronounced pulmonary immune response characterized by increased levels of pro-inflammatory cytokines and marked infiltration of immune effector cells in the lung tissues of rodent models (Vattanasit et al., 2023). Polystyrene (PS) is one of the "Big Five" polymers, alongside polyethylene (PE), polypropylene (PP), polyvinyl chloride (PVC), and polyethylene terephthalate (PET), which collectively dominate global plastic production and consumption (Singh et al., 2025). PS particles have been detected in human lung tissue (Amato-Lourenço et al., 2021) and have been implicated in the activation of inflammatory signalling pathways and the induction of cellular stress in response to MNPL exposure (Jiang et al., 2024; Siddiqui et al., 2023; Milillo et al., 2024; Bruno et al., 2024). Nevertheless, research investigating the impact of PS plastics (especially NPs) on airway and alveolar epithelial cells remains limited. Progress in NP toxicology research is hindered by the scarcity of in vitro models that accurately recapitulate the structural and physiological complexity of the human airway epithelium. Existing studies primarily rely on submerged monocultures of bronchial and alveolar epithelial cell lines, which are an accessible and cost-effective approach, albeit with several methodological constraints (Kouthouridis et al., 2021; Place et al., 2017). Altogether, these limitations underscore the need for more physiologically relevant in vitro models. Among them, Air-Liquid Interface (ALI) cultures are well-recognized three-dimensional (3D) cell models that more closely resemble in vivo airway exposure by realizing a direct contact between airborne particles and the apical cell surface (Lacroix et al., 2018; López-Rodríguez et al., 2018; López-Rodríguez et al., 2021a). On the other hand, owing to their small size and remarkable ability to interact with biological systems, NPs have recently attracted attention for their potential to affect cellular processes, similar to other nanoscale particles. In this framework, extracellular vesicles (EVs), lipid bilayer membranous vesicles secreted by virtually all cell types, are emerging as critical mediators of intercellular communication (Dellar et al., 2022). Conventionally, they were classified into three main types based on their biogenesis: exosomes (40–120 nm), microvesicles (50–1000 nm), and apoptotic bodies (500–2000 nm) (Welsh et al., 2024). More recently, additional EV subtypes have been identified, including oncosomes, which originate from membrane blebs in cancer cells (Ciardiello et al., 2019), and migrasomes. These vesicle-like structures form on the retraction fibers of migrating cells (Fan et al., 2022) and have been implicated in several biological processes, such as immune regulation, tissue repair, and cancer metastasis (Zhai et al., 2023). These different EV subtypes often exhibit overlapping sizes and phenotypic features, making classification based on biogenesis challenging and potentially misleading (Théry et al., 2018). Thus, the International Society for Extracellular Vesicles (ISEV) has recommended the general use of the term "extracellular vesicles" for all subtypes, advocating a simplified classification based on size. In line with ISEV guidelines, EVs are now broadly categorized as small EVs (under 200 nm in diameter) and medium/large EVs (over 200 nm) (Théry et al., 2018; Welsh et al., 2024).

EVs facilitate intercellular communication by transferring a wide range of biomolecules, including proteins, lipids, mRNAs, and microRNAs, that orchestrate critical functions in recipient cells involved in immunity, inflammation, and tissue regeneration (Welsh et al., 2024; Dellar et al., 2022). Recently, the potential role of EVs in modulating the cell responses to environmental stressors, including MNPLs, has been suggested (Mierzejewski et al., 2023). Furthermore, MNPLs and EVs are increasingly recognized as key players in disease development linked to environmental contamination (Calzoni et al., 2024). Thus, the investigation of their interactions represents a highly compelling and emerging field of research.

In this study, we employed a human lung adenocarcinoma cell line (Calu−3) under ALI conditions to investigate the impact of PS-NPs on airway epithelial cell viability, barrier integrity, and cytokine secretion, as well as their potential to interfere with EV-mediated communication. Using this physiologically relevant lung epithelial model, this study provides valuable insights into the respiratory hazards of PS-NP exposure and their potential impact on epithelial barrier function and EV-mediated communication.

2. Methods

2.1. Physicochemical characterization of PS-NPs

PS-NPs (cat. # PS02002, manufacturer-reported mean diameter 40 nm) were obtained from Bangs Laboratories (Indiana, USA) and characterized by dynamic light scattering (DLS) and electrophoretic light scattering. Hydrodynamic diameter (Z-average), polydispersity index (PDI), and zeta potential were measured using a Malvern Zetasizer Nano ZS instrument (He–Ne laser, 633 nm; backscattering angle 173°) at 25 °C, at the Spectroscopic and Correlation Unit (CAI Chemical Technologies), Microanalytical Service of the Complutense University of Madrid (Spain). Measurements were performed on the as-supplied stock suspension (SS) and after dilution in phosphate-buffered saline (PBS). Size and PDI were determined by DLS, while zeta potential was measured by electrophoretic light scattering.

Dragon-green-labeled PS-NPs (Bangs Laboratories Inc., Cat # FSDG001, Lot 15738) were characterized by the manufacturer using photon correlation spectroscopy/quasi-elastic light scattering (PCS/QELS). According to the certificate of analysis, the mean hydrodynamic diameter of this batch was 44 nm. PS-NPs and Dragon-green-labeled PS-NPs were diluted to the desired final concentrations in PBS for cell treatments.

2.2. In vitro PS-NP exposure in a Calu−3 Air–Liquid Interface model during epithelial barrier establishment

An in vitro airway epithelium model based on the human lung adenocarcinoma Calu−3 cell line (ATCC, Ref. HTB−55, Manassas, VA, USA), growth at ALI, was employed as previously described (López-Rodríguez et al., 2021a; López-Rodríguez et al., 2021b). Briefly, Calu−3 cells were cultured on transwell supports (pore size 0.4 mm,

Corning, New York, USA), with a density of 3×10^5 cells/cm^2 in Dulbecco's Modified Eagle Medium/Nutrient Mixture F−12 (DMEM/F−12, Gibco, Thermo Fisher Scientific, Waltham, MA, USA) supplemented with 10% (v/v) heat-inactivated fetal bovine serum (FBS, Gibco, Thermo Fisher Scientific), two mM L-glutamine, 100 μg/mL penicillin, and 100 μg/mL streptomycin, by adding 100 μL and 500 μL of complete medium to the apical and basolateral side, respectively, at 37°C and 5% CO_2. Once 80% confluence was reached (about 2 days under submerged conditions), Calu-3 cells were cultured under ALI conditions for 7 days to establish the Calu−3 cell functional barrier (Fig. 1A). ALI condition culture was established by removing the apical side culture medium, while on the basolateral side, the culture medium was replaced with DMEM supplemented with 5% (v/v) FBS, 100 μg/mL penicillin, and 100 μg/mL streptomycin, and replaced every 2 days. Under ALI conditions, Calu−3 cells undergo different stages of epithelial development, ranging from immature/non-polarized (day 2) to mature/polarized (day 7) states (López-Rodríguez et al., 2021a, 2021b) (Fig. 1A). In the present study, ALI-cultured Calu−3 cells were therefore apically exposed to PS-NPs (12 and 120 μg/cm^2) or PBS (CTR) for 5 consecutive days (120 h), starting on day 2 and continuing through day 7, corresponding to the period in which the epithelium remains immature and undergoes progressive stabilization under ALI conditions (López-Rodríguez et al., 2021a, 2021b). The selected PS-NP concentrations were based on preliminary results obtained from a 3-(4,5-dimethylthiazol−2-yl)−2, 5-diphenyl-2H-tetrazolium bromide (MTT) cell viability assay performed on Calu−3 cells under submerged culture conditions (Supplementary Methods and Supplementary Fig. 1).

2.3. LDH assay

Because the MTT assay is not readily applicable to ALI cultures, cell damage was evaluated by quantifying lactate dehydrogenase (LDH) release using the CytoTox 96® Non-Radioactive Cytotoxicity Assay (Promega, Italy), according to the manufacturer's instructions. Briefly, Calu−3 cells were cultured under ALI conditions and exposed apically to PS-NPs as described above. Baseline LDH release (T0) was determined from apical washes and basolateral medium collected immediately before exposure. These samples were clarified by centrifugation to remove cellular debris prior to LDH quantification. Cultures were then maintained at ALI and treated for 5 days (120 h). To restrict measurements to the final 24 h of exposure, both compartments were refreshed at 96 h. At 120 h, media were collected, clarified by centrifugation to remove debris, and LDH levels were quantified spectrophotometrically at 490 nm following the manufacturer's protocol. For each insert, apical and basolateral absorbance values were measured separately and combined to obtain the total LDH release per well, accounting for compartment volumes. LDH values, therefore, were reported as volume-corrected absorbance at 490 nm (OD490), proportional to total extracellular LDH activity. Finally, because our experimental model relies on early-stage ALI cultures that are still undergoing physiological maturation and therefore exhibit inherently elevated spontaneous LDH release (He et al., 2021), treatment effects were expressed as $\Delta LDH = LDH_{120\,h} - LDH_{T0}$. Compartment-specific LDH values were also retained to allow descriptive assessment of LDH distribution across the epithelial barrier by calculating the apical-to-basolateral LDH ratio.

2.4. Assessment of transepithelial electrical resistance

Transepithelial electrical resistance (TEER) values of ALI-cultured Calu−3 cells were monitored using an EVOM2 voltmeter (World Precision Instruments, WPI, Sarasota, FL, USA) with STX2 electrodes, according to the manufacturer's instructions. Briefly, Calu−3 cells were cultured under ALI conditions and monitored every day for 7 days. Eight individual transwell supports were used for each group, and triplicate measurements were performed for each well. TEER values were expressed in Ω x cm^2 and calculated after correction using a blank (cell-free membrane to assess intrinsic resistance) and multiplying by the effective growth area (0.33 cm^2) (López-Rodríguez et al., 2021a; López-Rodríguez et al., 2021b; Srinivasan et al., 2015).

2.5. E-cadherin and ZO−1 localization and protein expression analysis

Localization and expression of E-cadherin and zonula occludens 1 (ZO−1), canonical proteins of adherens junctions (AJs) and tight junctions (TJs), respectively (Fiegel et al., 2003), were evaluated by confocal laser scanning microscopy (CLSM) (López-Rodríguez et al., 2021b) and by western blot (Giuliani et al., 2015; Saul et al., 2019; D'Agostino et al., 2021) as reported in Supplementary Methods.

2.6. Cytokine analysis

Apical and basolateral media from cells exposed to PS-NPs (120 μg/cm^2) or PBS (CTR) were analyzed by using the commercially available Human Cytokine Array C5 (Cat. n°. AAH-CYT−5–2, RayBiotech, Peachtree Corners, GA, USA), a multiplex membrane-based antibody array for the semi-quantitative detection of 80 proteins, as previously described (Tang et al., 2025; López-Rodríguez et al., 2018). Chemiluminescent signals were analyzed using the LAS−3000 Mini Imaging System (Fujifilm), and optical density signals were quantified by using ImageJ software (NIH), normalized to internal positive controls, and expressed as fold changes, where fold change represents the relative expression of PS-NPs 120 μg/cm^2 compared to control. The heatmap was generated using GraphPad Prism (GraphPad Software, version 9, San Diego, CA).

2.7. Ingenuity pathway analysis

Based on the results of semi-quantitative cytokine array in ALI-cultured Calu−3 cells exposed to PS-NPs (120 μg/cm^2) vs CTR, the corresponding gene list (Supplementary Table 1) that contains gene symbols and corresponding expression values (fold-change>1.5) was uploaded into the Ingenuity pathway analysis (IPA) software (QIAGEN, Hilden, Germany), and the source of the organism was filtered by "Homo Sapiens" to generate a human molecular interaction pathway. Then, the core analysis in IPA was used to analyze the functional analysis, such as canonical pathways and upstream regulators. The significance of the association between the uploaded dataset and a canonical pathway was determined by a *p*-value of overlap calculated by a right-tailed Fisher's exact test. All enriched pathways were sorted from largest to smallest by Z-score values.

The upstream regulator analysis was used to evaluate the observed expression of the downstream genes in the uploaded dataset and to identify the putative regulators that contribute to the changes in gene expression in the significantly perturbed pathway. All analyses were based on the latest version of the Ingenuity database released in May 2025.

2.8. Cytokine validation

The Osteopontin (OPN) protein concentration in the culture media was analyzed using a commercial OPN ELISA kit (catalog number BMS2066; Thermo Fisher Scientific, Waltham, MA, USA) according to the manufacturer's protocol.

A panel of 12 cytokines was evaluated using a Milliplex custom kit for Luminex MAGPIX detection system (Affymetrix, eBioscience), following the manufacturer's instructions. Cytokine concentrations were normalized to the number of viable cells present at the end of the exposure period (120 h of ALI culture) and are reported as pg/mL per 10^5 viable cells. Viable cells were identified by exclusion of 7-aminoactinomycin D (7-AAD; BD Biosciences) and counted by flow-cytometry.

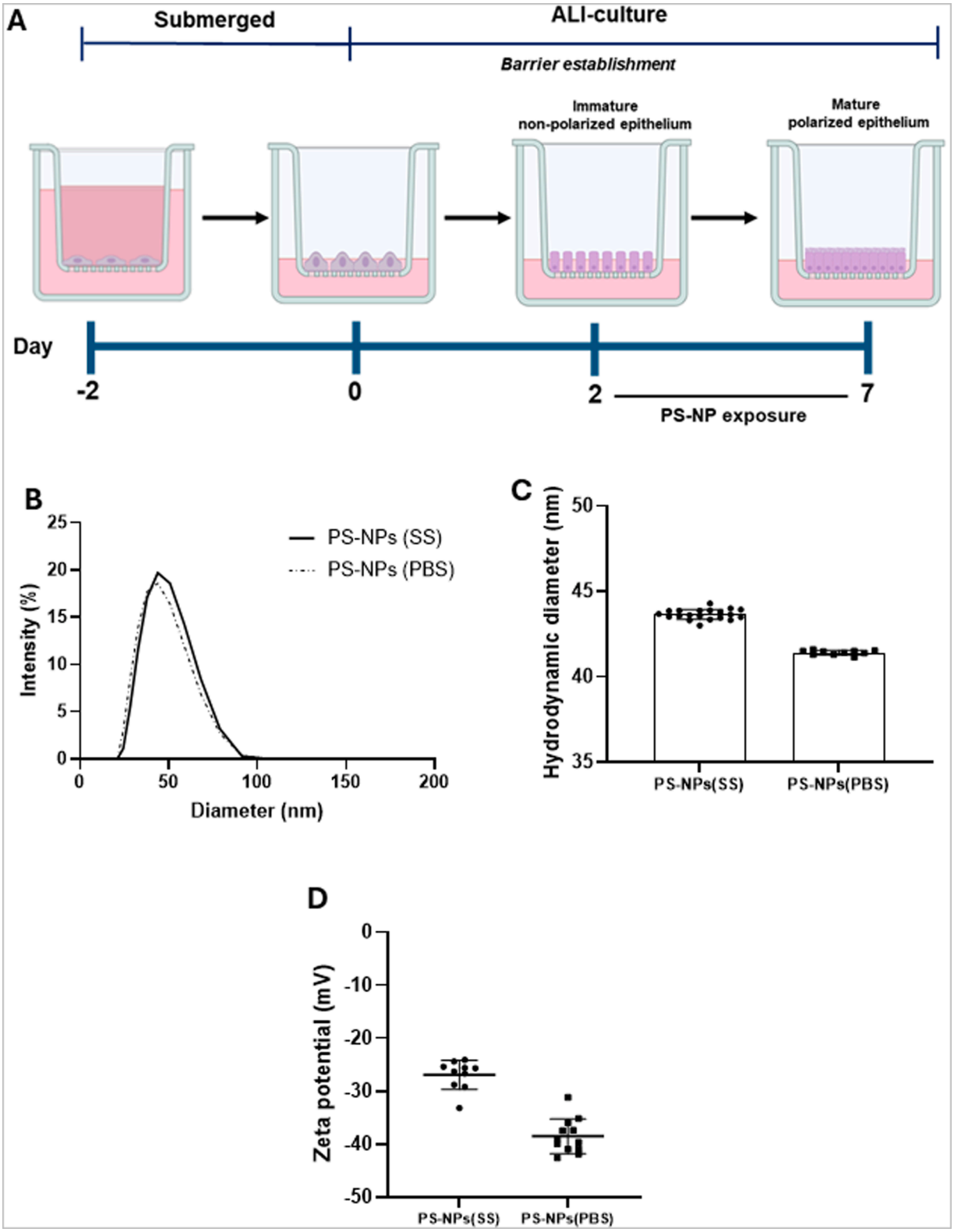

Fig. 1. Schematic representation of the three-dimensional (3D) in vitro model of Air-Liquid Interface (ALI) cultured Calu−3 cells and physicochemical characterization of polystyrene nanoplastics (PS-NPs, 40 nm) under exposure-relevant conditions (A) Calu−3 cells (3×10^5 cells/cm^2) were cultured submerged on transwell cell culture supports. After 2 days, once 80% confluence was reached, the culture medium was removed from the apical side, thus establishing the ALI condition (day 0), and the basolateral medium was changed with DMEM supplemented with 5% (v/v) FBS. Calu-3 cells were cultured under ALI conditions for 7 days to establish the Calu−3 cell functional barrier. This model at day 2 represents a functionally immature and more vulnerable airway epithelial barrier, whereas by day 7 it resembles a mature airway epithelium. From day 2 to day 7 (for a total duration of 120 h), cells were exposed to PS-NPs. (B) Intensity-weighted hydrodynamic size distributions measured by dynamic light scattering (DLS) for PS-NPs in stock suspension (SS) and after dilution in PBS, the exposure medium used for bronchial epithelial cells. (C) Z-average hydrodynamic diameter and (D) zeta potential measured by DLS and electrophoretic light scattering, respectively. Data are shown as individual measurements with mean ± SD.

2.9. Flow cytometry analysis of EVs

In Calu−3 cells cultured under ALI conditions and exposed to PS-NPs (12 and 120 μg/cm^2) or PBS (CTR) for 120 h, starting on day 2, apical and basolateral media samples were collected and stained to detect EVs as previously described and strictly adhering to MIFlowCyt-EV guidelines (Lanuti et al., 2025; Marchisio et al., 2020; Simeone et al., 2020; Welsh et al., 2020). Briefly, 100 μl of culture medium was added to 100 μl of 1x PBS, then stained using the reagents detailed in Supplementary Table 2 for 45 min, at RT, in the dark. For EV intravesicular staining, samples were fixed and permeabilized using 200 μl of Cytofix/Cytoperm (BD Biosciences, New Jersey) for 20 min at RT, in the dark, and stained with anti-Flotillin−1 antibody for 30 min (Supplementary Table 2). Samples were acquired by flow cytometry (Symphony A5, BD Biosciences) and analyzed for EV concentrations and phenotypes, as previously described (Lanuti et al., 2025; Marchisio et al., 2020; Simeone et al., 2020; Contursi et al., 2023) and reported in supplementary methods. The gating strategy used to identify EVs is depicted in Supplementary Fig. 2.

2.10. Statistical analysis

The data were analyzed using the Student's *t*-test or one-way ANOVA followed by Tukey's multiple comparisons test, or Kruskal–Wallis test, followed by Dunn's post hoc test with a Bonferroni correction for pairwise comparisons. All quantitative results were analyzed using GraphPad Prism Software (version 9.00 for Mac; GraphPad, San Diego, CA, USA). Data are presented as means ± standard error of the mean (SEM), unless otherwise specified, of at least three separate experiments. Values of $p \leq 0.05$ were considered statistically significant.

3. Results

3.1. Physicochemical characterization of PS-NPs

PS-NPs (manufacturer-reported mean diameter 40 nm) were characterized by DLS and electrophoretic light scattering to verify particle behavior under the experimental exposure conditions. Intensity-weighted size distributions showed a predominantly monomodal population with hydrodynamic diameters centered around 43–45 nm, both in SS and after dilution in PBS, the exposure medium used for bronchial epithelial cells (Fig. 1B). Quantitative analysis of the Z-average hydrodynamic diameter confirmed comparable particle sizes in SS and PBS, with low variability across independent measurements (Fig. 1C). PDI values remained low, indicating a narrow size distribution (Supplementary Table 3). Zeta potential measurements revealed negatively charged PS-NPs under both conditions, with more negative values observed in PBS compared to SS, consistent with ionic strength–dependent surface charge screening (Fig. 1D). Although characterization was performed in PBS to reproduce the defined exposure conditions used for ALI cultures, interactions with biological components released by epithelial cells during exposure cannot be excluded and may further influence NP surface properties. Overall, these results indicate that PS-NPs maintained stable colloidal behavior without detectable aggregation under the experimental exposure conditions.

3.2. Effect of PS-NP exposure on epithelial barrier establishment in ALI-cultured Calu−3 cells

Based on preliminary MTT assays performed in Calu−3 cells under submerged conditions (Supplementary Fig. 1), two PS-NP concentrations were selected to assess their impact on epithelial barrier establishment in ALI-cultured Calu−3 cells. Specifically, 12 μg/cm^2 was chosen as a concentration that preserved cell viability, whereas 120 μg/cm^2 was selected as a sub-lethal, stress-inducing dose approximating a worst-case exposure scenario (Supplementary Fig. 1).

Because the MTT assay is not readily applicable to ALI cultures, cell damage under ALI conditions was assessed by measuring total LDH release, combining apical and basolateral LDH values (Fig. 2A). At baseline (T0), Calu−3 cultures displayed relatively high spontaneous LDH release, consistent with the early maturation phase of ALI culture and ongoing epithelial remodeling (He et al., 2021). CTR cultures exhibited a negative ΔLDH over the final 24 h of exposure, indicating a progressive reduction in LDH release under ALI conditions. Exposure to 12 μg/cm^2 PS-NPs did not significantly affect ΔLDH compared with CTR. In contrast, 120 μg/cm^2 induced a significant increase in ΔLDH, reflecting enhanced cell damage during the last 24 h of treatment (Fig. 2A).

Since apical and basolateral fractions were collected separately throughout the experiment, the apical-to-basolateral LDH ratio was calculated as a descriptive measure of barrier polarization (Michi and Proud, 2021). Upon PS-NP exposure, a concentration-dependent decrease in the apical/basolateral LDH ratio was observed (Supplementary Table 4), suggesting an alteration in LDH compartmentalization across the epithelial layer, which may be indicative of impaired barrier integrity (Rezaee and Georas, 2014). Given these results and the fact that LDH release reflects loss of membrane integrity (Schlinkert et al., 2015), we further investigated epithelial barrier functionality by assessing TEER, a widely used quantitative technique for evaluating the integrity of TJ dynamics in cell culture systems of endothelial and epithelial monolayers (Srinivasan et al., 2015). The establishment of the epithelial barrier was daily monitored by TEER measurements, starting from day 2 in the ALI condition (Fig. 2B). At this time point (0 h), the epithelial barrier was still forming, as indicated by the low TEER value (approximately 104 Ω.cm^2) (Fig. 2B). Control cells showed a significantly increased in TEER value at 48 h, reaching values of 456 Ω.cm^2 after 120 h, which indicates the establishment of an epithelial barrier by day 7 through the formation of an apical junctional complex (Srinivasan et al., 2015; Lee et al., 2021; López-Rodríguez et al., 2021a; López-Rodríguez et al., 2021b).

Exposure to PS-NPs (12 and 120 μg/cm^2) for 48 h or longer significantly reduced TEER values compared to control cells in a concentration-dependent manner, thus suggesting an impairment of epithelial barrier establishment. CLSM analyses supported these results. As shown in Fig. 2C, ALI-cultured Calu−3 cells exposed to PS-NPs for 120 h exhibited a concentration-dependent decrease in the fluorescence intensity of the AJ protein E-cadherin and TJ protein ZO−1, which contribute to the apical junctional complexes (AJCs) (Shaykhiev et al., 2011). Moreover, an altered distribution pattern of both proteins, characterized by a disrupted and discontinuous ring at the cell–cell junctions, was observed (Fig. 2C). The decreased expression levels of E-cadherin and ZO−1 were confirmed by western blot analysis and the corresponding OD measurements (Fig. 2D-E and Supplementary Fig. 3). Collectively, these findings suggest that PS-NP exposure impairs epithelial barrier establishment by affecting both ZO−1 and E-cadherin, likely increasing paracellular permeability and altering the barrier function of the bronchial epithelium.

3.3. Exploratory cytokine profiling following PS-NP exposure in early-stage ALI-cultured Calu−3 cells

To obtain an exploratory overview of cytokine modulation induced by PS-NP exposure and to guide subsequent quantitative analyses, a semi-quantitative human cytokine antibody array was performed using pooled conditioned media collected from the apical and basolateral compartments of early-stage ALI-cultured Calu−3 cells exposed for 120 h to the highest PS-NP concentration (120 μg/cm^2) or PBS (CTR).

Array profiling revealed broad cytokine modulation, with 22 and 36 cytokines showing relevant changes (fold change >1.5) in the apical and basolateral compartments, respectively (Supplementary Table 1). Most altered cytokines were upregulated, suggesting an overall activation of secretory signaling rather than suppression. Only 10 cytokines were

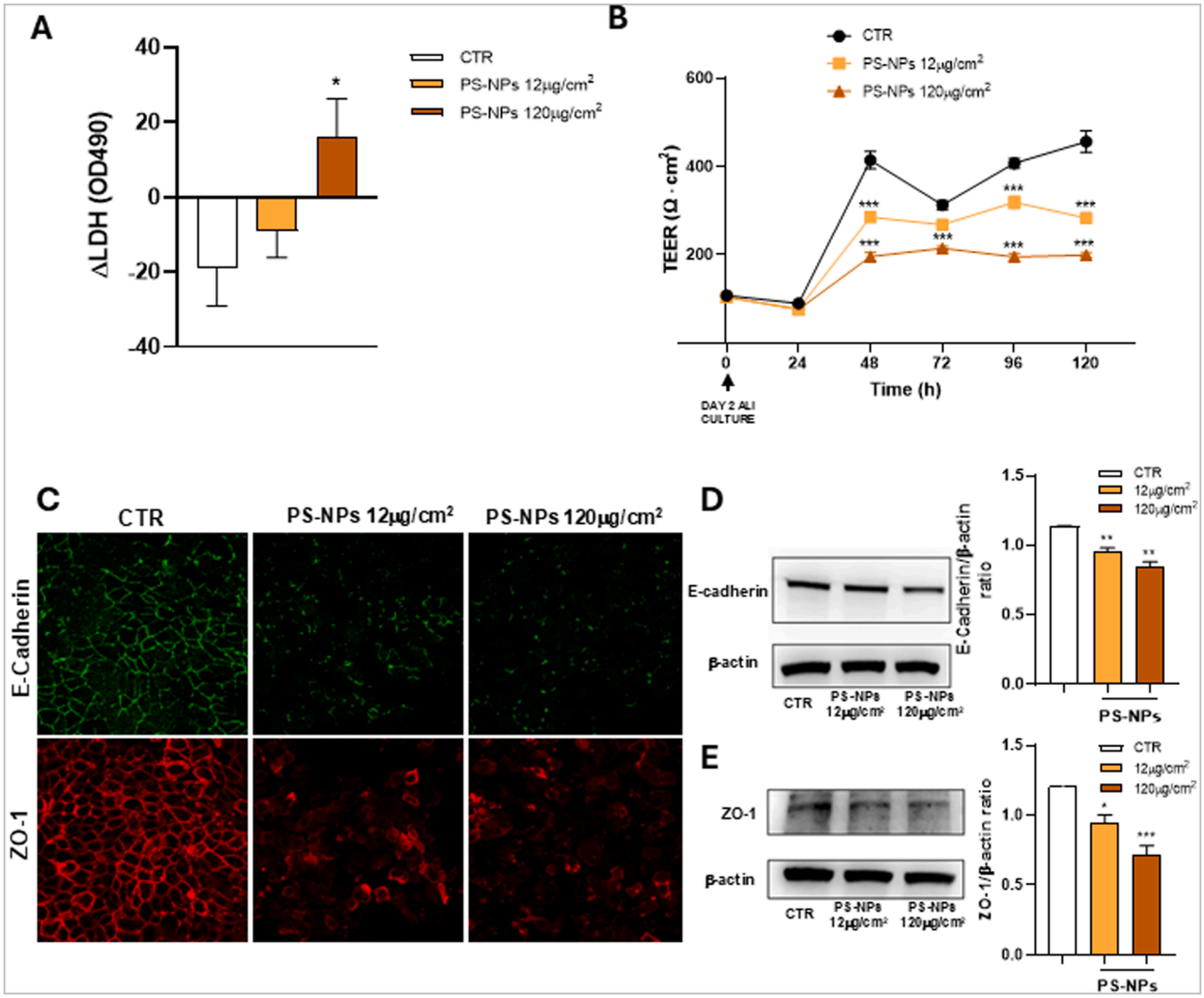

Fig. 2. Effects of PS-NPs (40 nm) on epithelial barrier integrity and junctional protein expression. (A) Calu−3 cells cultured under ALI conditions were exposed apically to PS-NPs (12 and 120 μg/cm^2) for 120 h. Cell membrane damage was assessed by measuring total LDH release (apical + basolateral). To account for the elevated spontaneous LDH release of early-stage ALI cultures, data are expressed as ΔLDH, calculated as the change in total LDH signal between 120 h and baseline (T0). LDH values represent volume-corrected absorbance at 490 nm (OD490). Values represent the mean ± SEM (N = 4, each performed in duplicate). *P < 0.05 vs CTR. (B) Calu-3 cells (3 ×10^5 cells/cm^2) were cultured under ALI conditions and apically exposed to PS-NPs (diameter 40 nm) at the concentrations of 12 and 120 μg/cm^2, or PBS (CTR) for 120 h. The TEER values were expressed in Ω x cm^2 after correction using a blank (cell-free membrane to assess intrinsic resistance) and the effective growth area (0.33 cm^2). Data shown are the mean ± SEM of eight independent determinations (n = 8). Triplicate measurements were taken daily from each well at all tested time-points. ***P < 0.001 vs CTR (one-way ANOVA followed by Tukey's multiple comparisons test). (C) Representative images of E-cadherin (green) and ZO−1 (red) protein expression and localization in control conditions (CTR) and in ALI-cultured Calu−3 cells exposed to NPs (12 and 120 μg/cm^2) for 120 h, by CLSM analysis. Representative Z-stacks are shown. (D) The protein expression of E-cadherin (C) and ZO−1 (D) was analyzed by Western blot in ALI-cultured Calu-3 cells exposed to PS-NPs (12 and 120 μg/cm^2) for 120 h; β-actin was used as protein loading control. The images are representative of three different experiments. *P < 0.05 vs CTR; **P < 0.01 vs CTR; ***P < 0.001 vs CTR (Student's *t*-test).

commonly modulated in both compartments, including angiogenin (ANG), C-X-C motif chemokine ligand 8 (CXCL8), C-X-C motif chemokine 5 (ENA−78), growth-regulated α-protein (GRO-α/CXCL1), GROα/β/γ, interleukin−2 (IL−2), monocyte chemoattractant protein−1 (MCP−1/CCL2), transforming growth factor beta−2 (TGFβ−2), tissue inhibitor of metalloproteinases−1 (TIMP−1), and osteopontin (OPN), indicating partially compartment-specific secretion patterns consistent with polarized epithelial responses.

Among shared mediators, differences in modulation magnitude were observed between compartments. ENA−78 showed stronger induction in the basolateral medium (6.65-fold increase, FI) compared with the apical compartment (1.63-FI), whereas TGFβ−2 displayed greater upregulation apically (4.73-FI vs 1.92-FI basolateral).

OPN, previously proposed as a biomarker of exposure to fine particulate matter (Ho et al., 2019), was markedly increased in both compartments (4.31-FI apical; 5.84-FI basolateral). Distinct compartment-specific responses were also observed, with IL−5 selectively increased apically and VEGFA detected only in the basolateral medium (Supplementary Table 1). Heatmap visualization confirmed clear differences in cytokine profiles between PS-NP-exposed and control cells (Fig. 3A).

Overall, the cytokine release pattern suggests that PS-NP exposure induces a selective and compartment-dependent inflammatory response rather than a widespread acute inflammatory activation, even under a worst-case exposure scenario.

To explore biological relationships among modulated cytokines,

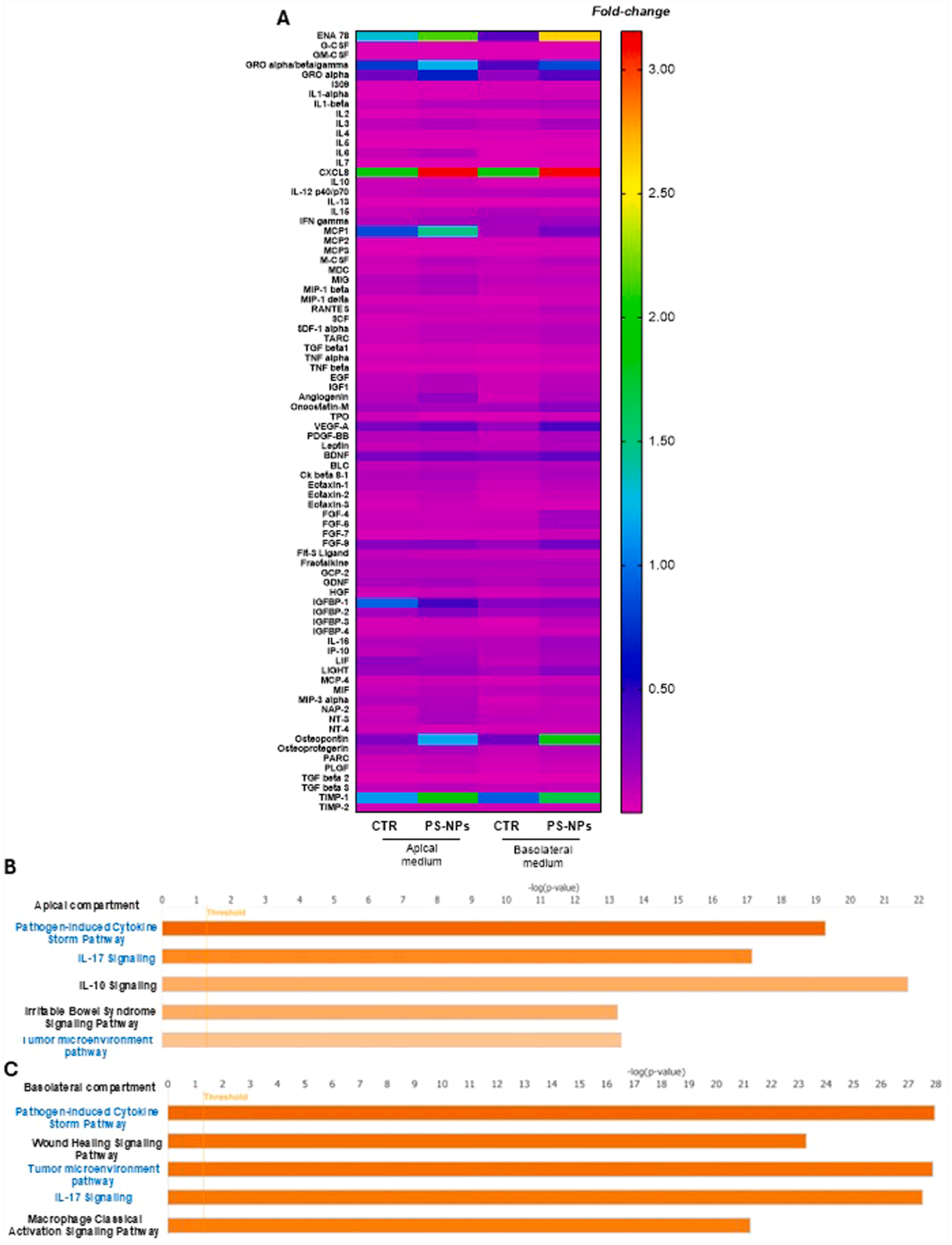

Fig. 3. Cytokine release in ALI-cultured Calu−3 cells exposed to PS-NPs: semi-quantitative array profiling and IPA-based pathway analysis. (A)Pooled samples of apical and basolateral media from ALI-cultured Calu−3 cells, exposed to PS-NPs (120 μg/cm^2) or PBS (CTR) for 120 h, were analyzed using a multiplex membrane-based antibody array for the semi-quantitative detection of 80 proteins. Signal intensities were normalized to internal positive controls, and expressed as fold changes, where fold change represents the relative expression of PS-NPs 120 μg/cm^2 compared to their relative control in apical and basolateral compartments, respectively. Data are reported as a heatmap. To investigate the biological pathways associated with PS-NP-induced cytokine modulation (120 μg/cm^2), cytokines showing fold-change values exceeding the predefined ±1.5 threshold in the apical and basolateral compartments were analyzed using Ingenuity Pathway Analysis (IPA), including canonical pathway enrichment analysis. Pathways significantly enriched ($p < 0.05$) among the cytokines altered in the apical (B) and basolateral (C) compartments were identified. The five most significantly enriched canonical pathways for each compartment are shown, ranked by Z score value. For canonical pathway analysis, the −log (P-value) of 1.30 was taken as the threshold.

datasets exceeding the ±1.5 fold-change threshold were analyzed using Ingenuity Pathway Analysis (IPA). Upstream regulator analysis identified OPN (gene name: SPP1), lipopolysaccharide (LPS), and cigarette smoke among the top predicted regulators in the apical compartment (Supplementary Fig. 4 A and Supplementary Table 5), while LPS and OPN were also prominent regulators in the basolateral compartment (Supplementary Fig. 4B and Supplementary Table 6). Canonical pathway enrichment highlighted inflammatory and stress-associated signaling networks, including the Pathogen-Induced Cytokine Storm pathway, tumor microenvironment signaling, and pathways related to IL−17-mediated inflammatory responses, in both the apical and basolateral compartments (Figs. 3B and 3C, respectively).

Given the semi-quantitative nature of the array analysis and its performance on pooled samples at a single exposure condition, selected cytokines emerging from this exploratory screening were subsequently subjected to targeted quantitative analyses to validate and refine PS-NP-induced secretion patterns across exposure concentrations.

3.4. *Quantitative assessment of cytokine secretion following PS-NP exposure in early-stage ALI-cultured Calu−3 cells*

Following exploratory cytokine array profiling, selected mediators were quantitatively assessed by using ELISA (for OPN) and Luminex multiplex technology (for ENA−78, IL−2, CXCL1, CCL2, TIMP−1, CXCL8, IL−1β, IFN-γ, IL−6, IL−10, VEGF, and IL−5). This cytokine panel was selected based on the microarray results and the availability of commercially validated assay kits, including pre-assembled multiplex panels from manufacturers.

In the apical compartment, PS-NP exposure significantly increased OPN secretion at both concentrations (12 and 120 μg/cm^2) compared with controls (Fig. 4A). Consistent increases were also observed for several pro-inflammatory and immunomodulatory cytokines, including IL−2, CXCL8, IL−1β, IFN-γ, and IL−10, which were elevated at both exposure levels (Fig. 4B-F). ENA−78 showed a significant increase at the lower concentration (12 μg/cm^2) (Fig. 4G), whereas IL−6 elevation was detected only at the higher concentration (120 μg/cm^2) (Fig. 4H). In contrast, CXCL1, CXCL2, and TIMP−1 did not show statistically significant changes (Supplementary Fig. 5).

In the basolateral compartment, quantitative analysis confirmed significant increases in OPN, IL−2, IL−10, and CXCL1 at both PS-NP concentrations (Fig. 5A–D). Additional cytokines, including ENA−78, TIMP−1, CXCL8, IL−1β, and CCL2, were significantly elevated only at the higher exposure condition (120 μg/cm^2) (Fig. 5E–I), suggesting a concentration-dependent amplification of basolateral signaling. No

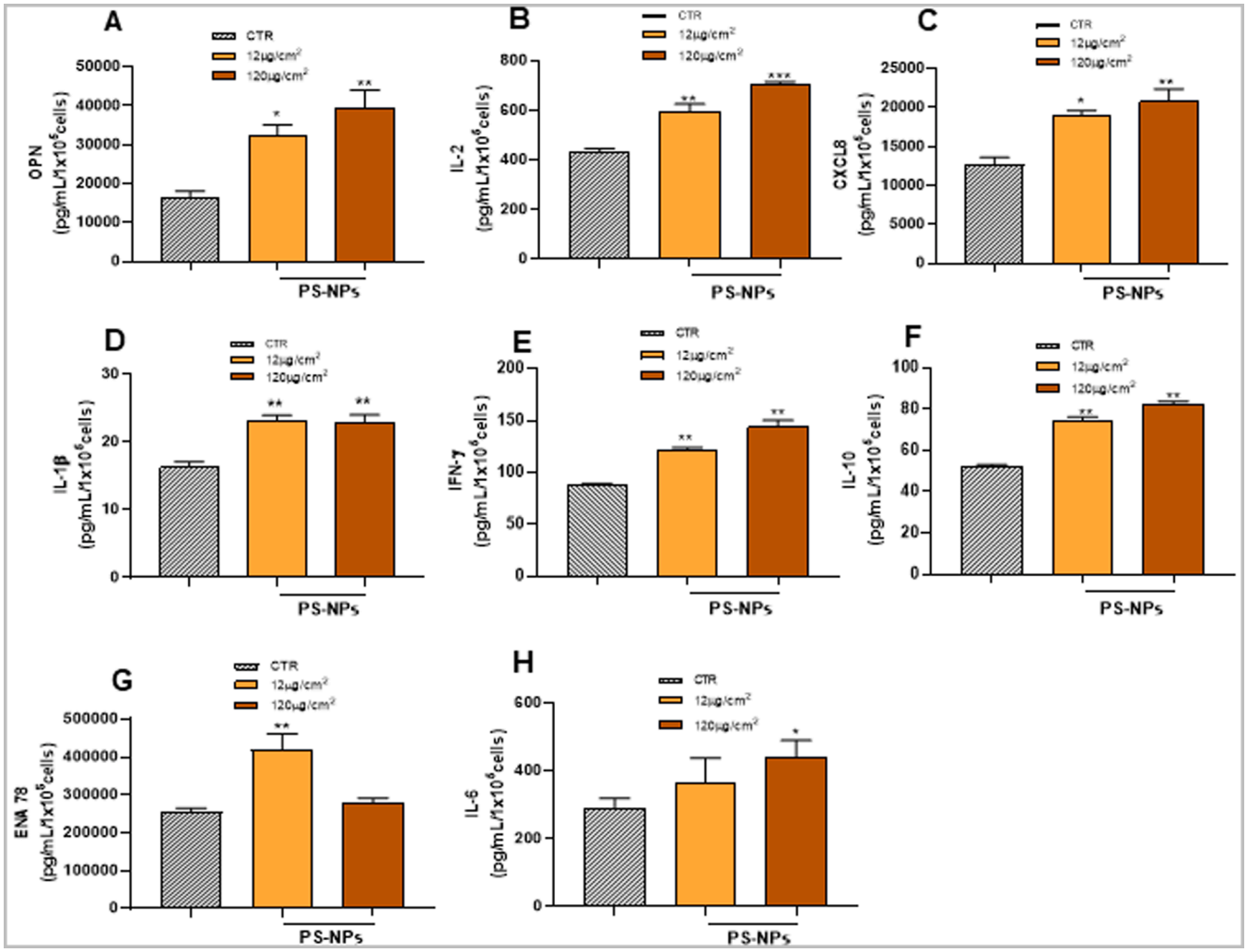

Fig. 4. Quantitative assessment of cytokines in apical medium of Air-Liquid Interface (ALI) cultured Calu−3 cells exposed to PS-NPs. Osteopontin (OPN) (A) levels in the apical of ALI-cultured Calu−3 cells exposed to PS-NPs (12 and 120 μg/cm^2) for 120 h were assessed by ELISA. Data shown are the mean ± SEM (n = 6–8), *P < 0.05 vs CTR and **P < 0.01 vs CTR (Student's *t*-test). The levels of IL−2 (B), CXCL8 (C), IL−1β (D), IFN-γ (E), IL−10 (F), ENA 78 (G), IL−6 (H), were assessed in the apical medium of ALI-cultured Calu−3 cells exposed to PS-NPs (12 and 120 μg/cm^2) for 120 h by a Luminex detection system. Cytokine levels were expressed as pg/mL *per* 10^5 viable cells. Data shown are the mean ± SEM (n = 4). (B-H) *P < 0.05 vs CTR and **P < 0.01 vs CTR (Student's *t*-test).

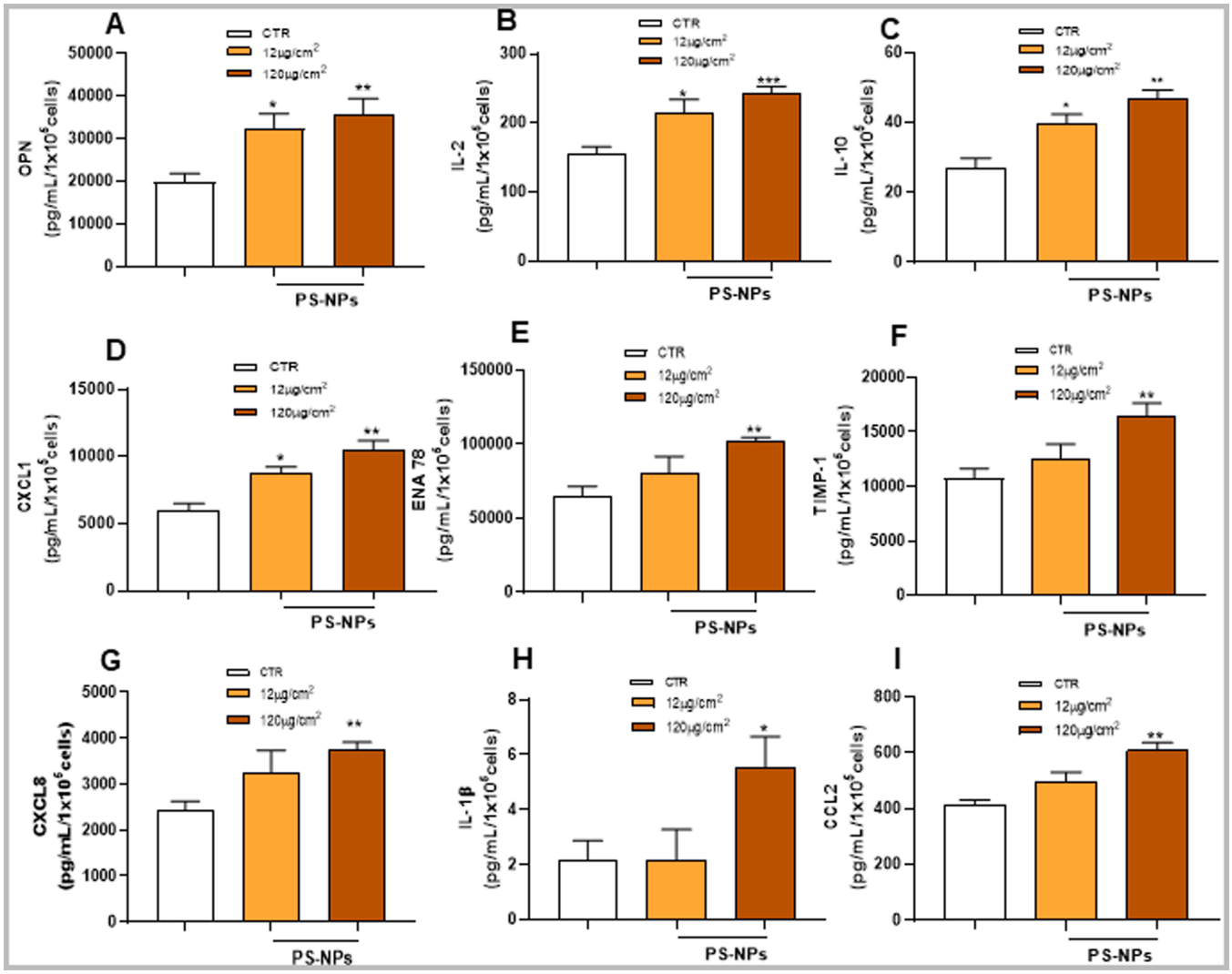

Fig. 5. Quantitative assessment of cytokines in basolateral medium of Air-Liquid Interface (ALI) cultured Calu−3 cells exposed to PS-NPs. Osteopontin (OPN) (A) levels in the basolateral compartment of ALI-cultured Calu−3 cells exposed to PS-NPs (12 and 120 µg/cm^2) for 120 h were assessed by ELISA. Data shown are the mean ± SEM (n = 6–8), *P < 0.05 vs CTR and **P < 0.01 vs CTR (Student's *t*-test). The levels of IL−2 (B), IL−10 (C), CXCL1 (D), ENA 78 (E), TIMP-1 (F), CXCL8 (G), IL−1β (H), and CCL2 (I) were assessed in the basolateral medium of ALI-cultured Calu−3 cells exposed to PS-NPs (12 and 120 µg/cm^2) for 120 h by a Luminex detection system. Cytokine levels were expressed as pg/mL *per* 10^5 viable cells. Data shown are the mean ± SEM (n = 4). (B-I) *P < 0.05 vs CTR and **P < 0.01 vs CTR (Student's *t*-test).

significant changes were observed for IL−6 or IFN-γ (Supplementary Fig. 6). VEGF and IL−5 levels remained below detection limits in both compartments.

Overall, quantitative analyses confirmed a selective increase in cytokine secretion following PS-NP exposure, characterized by compartment-dependent and partially concentration-dependent responses. Notably, OPN, IL−2, and IL−10 were consistently increased in both apical and basolateral compartments at both PS-NP concentrations, whereas other mediators displayed concentration- and compartment-specific secretion patterns.

3.5. PS-NP internalization and EV release following PS-NP exposure in early-stage ALI-cultured Calu−3 cells

To investigate whether the secretory alterations observed following PS-NP exposure could be associated with NP uptake and EV-mediated communication, the ability of early-stage ALI-cultured Calu−3 cells to internalize PS-NPs was first assessed by CLSM after exposure to dragon green–conjugated NPs (12 and 120 µg/cm^2) for 120 h (Fig. 6A–C). Green fluorescence was absent in CTR cells (Fig. 6A), but clearly detectable in exposed cells (Fig. 6B-C), confirming PS-NP internalization. Internalized NPs exhibited a predominantly perinuclear distribution, with accumulation increasing in a concentration-dependent manner.

Previous studies have shown that PS-NP exposure can stimulate EV release in different cell types, including astrocytes and macrophages (Adamiak et al., 2024; Deville et al., 2022). Therefore, in media collected from cells exposed to PS-NPs (12 and 120 µg/cm^2), we assessed EV concentrations both in apical and basolateral compartments by flow cytometry. The entire populations of EVs released from unexposed cells (CTR, Supplementary Fig. 7A-B), as well as from cells exposed to PS-NPs 12 µg/cm^2 (Supplementary Fig. 7C-D) and 120 µg/cm^2 (Supplementary Fig. 7E-F), expressed both CD63 and FLOT−1, two canonical EV markers recommended by the current MISEV guidelines for EV characterization (Welsh et al., 2024). These findings confirm the vesicular nature of the analyzed particles. We observed 100% positivity for both markers under all conditions analyzed, as demonstrated by a complete shift in the fluorescence signal of the stained samples (blue histograms) compared to the respective FMO controls (red histograms), and by MFI ratio values, all of which were

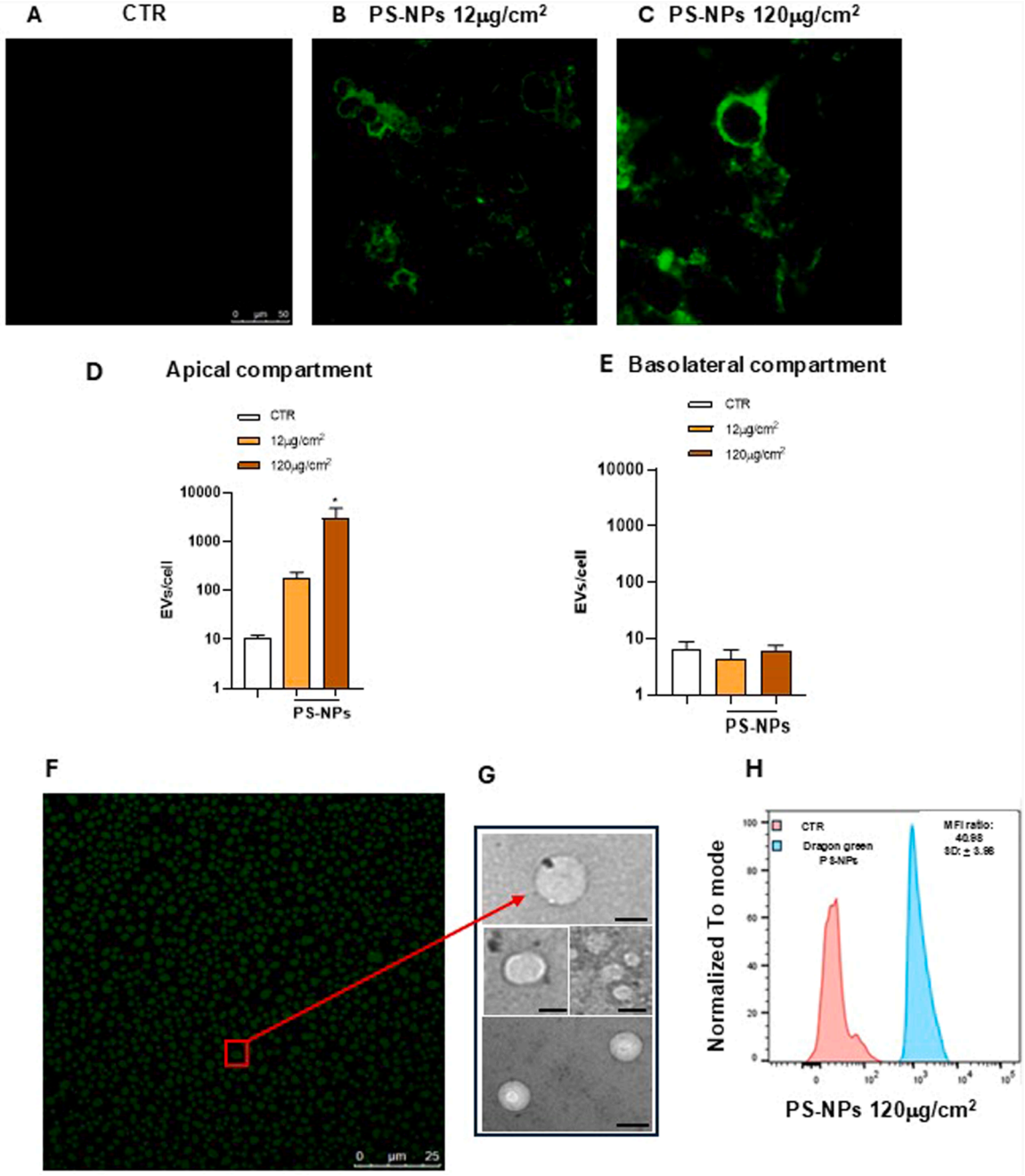

Fig. 6. PS-NPs internalization and release of EVs generated by Air-Liquid Interface (ALI) cultured Calu−3 cells exposed to PS-NPs. ALI-cultured Calu−3 cells were unexposed (A) or exposed to Dragon green-labelled PS-NPs at 12 µg/cm^2 (B) or 120 µg/cm^2 (C) for 120 h. Representative images of green-fluorescent PS-NP cell internalization. EVs released from apical (D) and basolateral (E) compartments of cells were quantified using a volumetric counting device. The Y-axis shows the number of EVs per cell (EVs/Cell), calculated by normalizing measured EV concentrations to the number of corresponding parental viable cells. Data shown are the mean ± SEM (n = 3). (D-E) *P < 0.05 vs CTR [one-way ANOVA (Kruskal–Wallis) with Dunn–Bonferroni post hoc test]. PS-NP incorporation into EVs released by ALI cultured Calu−3 cells was evaluated by sorting and isolated EVs were from apical compartment of ALI-cultured Calu−3 cells exposed to Dragon green (FITC)-labelled PS-NPs (12 and 120 µg/cm^2). Representative image of green-fluorescent PS-NPs incorporated into EVs by CLSM (F). Representative images of isolated EVs by TEM (scale bar: 100 nm) (G). Flow cytometry analysis of isolated EVs released from Calu−3 cells unexposed or exposed to Dragon green (FITC) -labelled PS-NPs (H). Blue histogram represents the fluorescence signal (FITC channel) of PS-NPs contained within isolated EVs released by cells exposed to PS-NPs (Dragon-green PS-NPs). The overlaid red histogram represents EVs from untreated cells (CTR). Data are representative of three independent experiments.

greater than 2.

During the final 24 h of exposure, EV secretion in the apical compartment showed a tendency to increase at 12 µg/cm^2, reaching statistical significance only at the highest concentration tested (120 µg/cm^2) (Fig. 6D), whereas no significant changes were detected basolaterally (Fig. 6E). Notably, EV numbers in the apical medium were one to two orders of magnitude higher than those detected basolaterally. Based on these findings, subsequent analyses were focused on apical EVs.

CLSM analysis demonstrated that apical EVs released by Dragon green-PS-NP-exposed Calu−3 cells clearly exhibited green fluorescence originating from the fluorescent dye conjugated to PS-NPs (Fig. 6F). TEM analysis confirmed their EV morphology and showed that they had a diameter of approximately 100 nm, surrounded by a cell membrane that may provide protection for their internal cargo (Fig. 6G). The flow

cytometry analysis confirmed that the entire apical EV population released by Dragon green-PS-NP-exposed Calu−3 cells (120 μg/cm^2 for 120 h) exhibited green (FITC) fluorescence (Fig. 6H, blue histogram), in contrast to EVs from unexposed CTR cells (Fig. 6H, red histogram).

Collectively, these results demonstrate that PS-NPs are efficiently internalized by ALI-cultured Calu−3 cells and promote a polarized increase in EV release, with NP incorporated into secreted vesicles. These findings support a potential role for EVs as carriers of internalized NPs, providing a mechanistic basis for PS-NP dissemination through epithelial communication pathways.

4. Discussion

During the last decades, the adverse effects of MNPLs on human health have become a growing global concern, largely because of their ability to cross biological barriers, accumulate intracellularly, and interfere with essential cellular functions (Bridgeman et al., 2025). Most in vitro studies investigating the effects of MNPLs on human respiratory health have relied on submerged-exposure models, which fail to recapitulate the structural and functional complexity of the airway epithelium (Wright et al., 2024). In contrast, ALI cultures provide a physiologically relevant system that promotes epithelial differentiation and polarization, barrier integrity, and mucus secretion (Silva et al., 2023; López-Rodríguez et al., 2018).

Among available in vitro models, Calu−3 cells represent one of the few human airway-derived epithelial lines capable of forming TJs and sustaining high TEER, thereby providing a reliable surrogate of the airway barrier. Under ALI culture conditions, this model recapitulates distinct stages of epithelial maturation: at day 2, the epithelium represents a functionally immature or compromised airway barrier. While it does not replicate the structural complexity of developing airway tissue in vivo, its high-permeability phenotype may model conditions characterized by impaired epithelial integrity, such as epithelial injury, repair, or inflammatory airway diseases. In contrast, by day 7 it closely resembles a mature and restrictive epithelial barrier (López-Rodríguez et al., 2018, 2021a, 2021b). Using this system, we show that chronic exposure to PS-NPs during the critical window of barrier establishment interferes with epithelial barrier formation and modulates immune signaling pathways. Importantly, these findings suggest that PS-NP exposure may exacerbate epithelial dysfunction in airway conditions characterized by incomplete or compromised barrier integrity, rather than merely damaging a fully mature epithelium.

Compared with our previous observations in submerged A549 cultures, in which PS-NPs induced oxidative stress, senescence, and apoptosis (Milillo et al., 2024), the present ALI-cultured Calu−3 model enabled investigation of additional features directly relevant to airway exposure, including epithelial barrier establishment, polarized cytokine secretion, and EV release. These characteristics support the physiological relevance of ALI-based airway models for studying the respiratory effects of inhaled NPs (Lacroix et al., 2018).

The integrity of the epithelial barrier relies on AJ and TJ proteins, which connect neighbouring cells and ensure proper cell polarization, an essential process for lung homeostasis (Hellings, Steelant, 2020; Pell et al., 2021). Disruption of this barrier by NP exposure has been linked to the onset and exacerbation of respiratory pathologies, including asthma, COPD, pulmonary fibrosis, and tumors (Gou et al., 2024). In our study, chronic exposure to PS-NPs impaired epithelial barrier establishment in a concentration-dependent manner, as demonstrated by reduced TEER values compared to unexposed cells.

CLSM analyses revealed altered distribution and reduced expression of E-cadherin and ZO−1, canonical proteins of AJs and TJs (Gao, Rezaee, 2022), respectively, and western blot analyses confirmed their downregulation during barrier establishment. These observations are consistent with previous reports showing that NPs compromise bronchial epithelial integrity through disruption of intercellular junctions (Srinivasan et al., 2015; Lee et al., 2021; López-Rodríguez et al., 2021a, 2021b; Hsu et al., 2025). These findings also align with the epithelial barrier theory, which proposes that chronic exposure to environmental barrier-disrupting agents contributes to inflammatory disease development (Akdis, 2021; Celebi Sozener et al., 2022).

Chronic PS-NP exposure promoted the release of multiple inflammatory mediators in early-stage ALI-cultured Calu−3 cells. Notably, OPN, IL−2, and IL−10 were consistently increased in both apical and basolateral compartments at both PS-NP concentrations, whereas other mediators displayed concentration- and compartment-specific secretion patterns. This polarized cytokine release suggests selective activation of epithelial signaling pathways and paracrine communication toward the submucosal milieu.

Among the altered cytokines, OPN may represent a relevant mediator, given the markedly elevated levels detected. OPN is a multifunctional glycoprotein involved in immune regulation and tissue remodeling processes (Du et al., 2022), including airway inflammation (Kohan et al., 2009), and its levels are increased in chronic airway diseases such as asthma, COPD, and idiopathic pulmonary fibrosis (Xu et al., 2019; Papaporfyriou et al., 2014; Pardo et al., 2005). Increased plasma OPN has also been associated with exposure to fine particulate matter in humans (Ho et al., 2019). In our study, OPN was predicted among upstream regulators together with canonical inflammatory triggers such as LPS and cigarette smoke, supporting the concept that PS-NP exposure activates signalling pathways resembling responses to environmental or infectious stressors.

IL−2 and IL−10 were also consistently secreted following chronic PS-NP exposure. Although IL−2 is traditionally associated with T-cell activation, epithelial-derived IL−2 has been reported under stress conditions (Aoki et al., 1997) and may contribute to immune cell recruitment and epithelial–immune crosstalk. Likewise, IL−10 secretion by airway epithelial cells has been described under oxidative and environmental stress (Latorre et al., 2014; Zhang et al., 2021) and may represent an epithelial regulatory response occurring in parallel with the production of pro-inflammatory mediators, including IL−1β, and CXCL8.

Although key mediators of the IL−17 axis, such as IL−17 and IL−23, were not directly quantified, several cytokines significantly modulated following PS-NP exposure, including IL−1β, CXCL8, and CXCL1, are known downstream effectors of IL−17-associated inflammatory responses (Margelidon-Cozzolino et al., 2022) and may have contributed to the enrichment of the IL−17 signaling pathway identified by IPA.

Together, these findings indicate that PS-NP exposure did not trigger a widespread or overtly cytotoxic inflammatory response; rather, it induced a selective, compartment-dependent modulation of several cytokines, suggesting activation of epithelial inflammatory signaling pathways.

Persistent cytokine production has been associated with tissue remodeling processes, including epithelial–mesenchymal transition (EMT) (Bruno et al., 2018; Dovizio et al., 2015; Johnson et al., 2011). In this context, the reduction in epithelial junctional proteins (E-cadherin and ZO−1), together with increased OPN expression, may indicate early molecular changes consistent with a pro-remodeling epithelial phenotype following chronic PS-NP exposure.

In this study, PS-NPs 40 nm were used. NPs smaller than 100 nm are widely present in urban air worldwide (Vouitsis et al., 2023), underscoring their environmental relevance for inhalation exposure. Particles within this size range more readily cross biological barriers, undergo cellular uptake, and reach intracellular compartments, increasing their potential for biological interference (Sousa de Almeida et al., 2021). Previous studies have also shown that Calu−3 cells may release internalized particles following uptake (Paget et al., 2015; Michelini et al., 2025), although the underlying mechanisms remain poorly understood.

The polarized cytokine secretion observed under ALI conditions prompted us to investigate whether NP uptake could influence intercellular communication mechanisms, particularly EV release. We demonstrate that chronic PS-NP exposure led to intracellular

accumulation, increased EV release, and active packaging of PS-NPs into EVs. To our knowledge, these findings provide further evidence supporting EV-mediated transport of NPs (Wang et al., 2024; Calzoni et al., 2024; Adamiak et al., 2024; Kim et al., 2024; Hsu et al., 2025). EV release may represent a protective cellular mechanism by sequestering NPs and limiting acute toxicity, consistent with the observed limited cytotoxicity under the tested exposure conditions. However, EVs are also active mediators of intercellular communication capable of transferring cytokines, miRNAs, and damage-associated molecular patterns (DAMPs) (Calzoni et al., 2024), suggesting that EV-mediated signaling may contribute to the propagation of NP-induced responses during chronic exposure. Although the present study demonstrates NP incorporation into EVs and increased vesicle release, the functional impact of these EVs on recipient cells was not directly addressed. The primary aim of this work was to characterize epithelial responses and EV-mediated NP trafficking under ALI conditions. Future studies will be required to determine whether EV-associated NPs can modulate signaling pathways in neighboring epithelial or immune cells and thereby contribute to propagation of NP-induced responses within the airway microenvironment.

Altogether our findings are consistent with recent studies showing that NP exposure under ALI conditions disrupts epithelial barrier integrity and promotes inflammatory responses in airway epithelial models (Alba García-Rodríguez et al., 2024; Michelini et al., 2025). These studies demonstrated reduced TJ integrity and activation of pro-inflammatory signalling following exposure to NPs in differentiated airway epithelia. While our study supports these observations, it extends current knowledge by investigating PS-NP exposure during epithelial barrier establishment, a vulnerable stage reflecting conditions of epithelial injury, repair, or pre-existing airway dysfunction. Moreover, we identified and validated OPN as one of the most consistently induced mediators following PS-NP exposure, supporting its potential relevance as a sensitive biomarker of NP-induced epithelial stress and remodeling. Finally, beyond barrier impairment and inflammatory mediator release, we demonstrate a polarized secretory response and identify EVs as potential carriers of internalized PS-NPs, suggesting an additional mechanism through which NPs may propagate biological effects within the respiratory microenvironment.

In our study, early-stage ALI-cultured Calu−3 cells were exposed to PS-NP concentrations of 12 and 120 μg/cm^2, which fall within exposure ranges commonly employed in in vitro nanotoxicology studies (Domenech et al., 2020) and are consistent with previous investigations using airway epithelial models (Lee, Rezaee, 2024). Accordingly with our previous studies, these concentrations were selected to cover exposure conditions ranging from levels potentially experienced in urban environments to higher exposure scenarios that may occur in occupational or industrial settings (Milillo et al., 2024). However, accurately quantifying airborne NP deposition and retained doses in the human respiratory tract remains technically challenging, particularly for nanosized particles, as exposure levels can currently only be extrapolated from datasets on larger sized particles and are highly variable among individuals (Grosselink et al., 2026). Consequently, as the purpose of this study was hazard characterization rather than risk assessment, in vitro concentrations exceeding estimated environmental levels were applied to enable identification of potential toxicological mechanisms, consistent with established practice in respiratory nanotoxicology (Domenech et al., 2020).

We showed that LDH release patterns is associated with minimal cytotoxicity at 12 μg/cm^2, whereas significant increases were observed only at 120 μg/cm^2, suggesting that these concentrations primarily modulate epithelial physiology and barrier function rather than inducing extensive cell death. The selected exposure range, therefore, enabled investigation of epithelial barrier disruption and inflammatory signaling under sustained NP exposure conditions while preserving sufficient epithelial integrity for mechanistic analyses. Taken together, although the concentrations used in the present study may not directly reproduce average human inhalation exposure levels, the higher concentration was included to model a worst-case or localized accumulation scenario in vulnerable airway epithelium undergoing barrier establishment under ALI conditions.

Some limitations should be acknowledged. Using a single epithelial cell line (Calu−3) does not fully capture the cellular complexity of the in vivo airway environment, particularly the contributions of immune and stromal components. In addition, downstream functional consequences of cytokine signaling were not directly assessed. The focus on early-stage ALI conditions was intended to model a vulnerable phase of epithelial barrier establishment, and findings cannot be directly extrapolated to fully mature airway epithelia; therefore, comparison with fully differentiated epithelia will be important in future studies. Finally, commercially available particles may not fully reproduce the physicochemical heterogeneity of environmental NPs.

In conclusion, chronic exposure to PS-NPs (40 nm) induces structural and functional alterations in ALI-cultured Calu−3 cells during epithelial barrier establishment, resulting in increased barrier vulnerability. These alterations include impaired barrier formation and selective, compartment-dependent inflammatory signaling. Furthermore, PS-NP exposure increased apical EV release and promoted incorporation of NPs into secreted vesicles. Collectively, these findings identify EV release as a potential mechanistic link between NP uptake and alterations in epithelial signaling. Future studies should characterize the molecular cargo of EVs released upon NP exposure and determine how NP-induced EV signaling influences airway epithelial communication pathways, potentially supporting the development of EV-based biomarkers of exposure.

CRediT authorship contribution statement

Sabrina Burattini: Investigation, Formal analysis. **Michela Battistelli:** Investigation, Formal analysis, Data curation. **Marco Gatta:** Investigation, Formal analysis. **Melania Dovizio:** Writing – review & editing, Writing – original draft, Formal analysis, Data curation, Conceptualization. **Elena Niccolai:** Methodology, Investigation, Formal analysis. **Jorge Parrón-Ballesteros:** Investigation, Formal analysis, Data curation. **Piero Di Carlo:** Writing – review & editing, Data curation. **Patrizia Ballerini:** Writing – review & editing, Project administration, Data curation, Conceptualization. **Francesca D'Ascanio:** Investigation, Formal analysis. **Amedeo Amedei:** Writing – review & editing, Investigation, Data curation, Conceptualization. **Annalisa Bruno:** Writing – review & editing, Writing – original draft, Formal analysis, Data curation. **Eva Batanero:** Writing – review & editing, Project administration, Methodology, Conceptualization. **Cristina Milillo:** Writing – original draft, Methodology, Investigation, Formal analysis. **Paola Lanuti:** Writing – review & editing, Writing – original draft, Formal analysis, Data curation.

Declarations

The authors used Grammarly Premium (V1.2.263.1893) to support language editing and improve clarity and grammatical accuracy.

Declaration of Competing Interest

The authors declare that they have no known competing financial interests or personal relationships that could have appeared to influence the work reported in this paper.

Acknowledgements

European Union—Next Generation EU—under the National Recovery and Resilience Plan (NRRP), Mission 4 Component 2 -M4C2, Investment 1.5—Call for Tender No. 3277 of 30 December 2021, Italian Ministry of University, Award No. ECS00000041, Project Title:

"Innovation, digitalization, and sustainability for the diffused economy in Central Italy", Concession Degree No. 1057 of 23 June 2022, adopted by the Italian Ministry of University. CUP: D73C22000840006; Ministry of Science and Innovation (Grant/Award Number PID2020–116692RB-I00).

Appendix A. Supporting information

Supplementary data associated with this article can be found in the online version at doi:10.1016/j.tox.2026.154533.

Data Availability

Data will be made available on reasonable request.

References

Adamiak, K., Sidoryk-Węgrzynowicz, M., Dąbrowska-Bouta, B., Sulkowski, G., Strużyńska, L., 2024. Plastic nanoparticles interfere with extracellular vesicle pathway in primary astrocytes. Ecotoxicol. Environ. Saf. 286, 117180. https://doi.org/10.1016/j.ecoenv.2024.117180.

Akdis, C.A., 2021. Does the epithelial barrier hypothesis explain the increase in allergy, autoimmunity and other chronic conditions? Nat. Rev. Immunol. 21, 739–751. https://doi.org/10.1038/s41577-021-00538-7.

Amato-Lourenço, L.F., Carvalho-Oliveira, R., Júnior, G.R., dos Santos Galvão, L., Ando, R.A., Mauad, T., 2021. Presence of airborne microplastics in human lung tissue. J. Hazard. Mater. 416, 126124. https://doi.org/10.1016/j.jhazmat.2021.126124.

Aoki, Y., Qiu, D., Uyei, A., Kao, P.N., 1997. Human airway epithelial cells express interleukin-2 in vitro. Am. J. Physiol. 272, 276–286. https://doi.org/10.1152/ajplung.1997.272.2.l276.

Bridgeman, L., Cimbalo, A., López-Rodríguez, D., Pamies, D., Frangiamone, M., 2025. Exploring toxicological pathways of microplastics and nanoplastics: insights from animal and cellular models. J. Hazard. Mater. 490, 137795. https://doi.org/10.1016/j.jhazmat.2025.137795.

Bruno, A., Dovizio, M., Milillo, C., Aruffo, E., Pesce, M., Gatta, M., et al., 2024. Orally ingested micro- and nano-plastics: a hidden driver of inflammatory bowel disease and colorectal cancer. Cancers (Basel) 16, 3079. https://doi.org/10.3390/cancers16173079.

Bruno, A., Dovizio, M., Tacconelli, S., Contursi, A., Ballerini, P., Patrignani, P., 2018. Antithrombotic agents and cancer. Cancers (Basel) 10, 253. https://doi.org/10.3390/cancers10080253.

Calzoni, E., Montegiove, N., Cesaretti, A., Bertoldi, A., Cusumano, G., Gigliotti, G., et al., 2024. Microplastic and extracellular vesicle interactions: recent studies on human health and environment risks. Biophysica 4, 724–746. https://doi.org/10.3390/biophysica4040047.

Celebi Sozener, Z., Ozdel Ozturk, B., Cerci, P., Turk, M., Gorgulu Akin, B., Akdis, M., et al., 2022. Epithelial barrier hypothesis: effect of the external exposome on the microbiome and epithelial barriers in allergic disease. Allergy 77, 1418–1449. https://doi.org/10.1111/all.15240.

Ciardiello, C., Leone, A., Lanuti, P., Roca, M.S., Moccia, T., Minciacchi, V.R., et al., 2019. Large oncosomes overexpressing integrin alpha-V promote prostate cancer adhesion and invasion via AKT activation. J. Exp. Clin. Cancer Res. 38, 317. https://doi.org/10.1186/s13046-019-1317-6.

Contursi, A., Fullone, R., Szklanna-Koszalinska, P., Marcone, S., Lanuti, P., Taus, F., et al., 2023. Tumor-Educated Platelet Extracellular Vesicles: Proteomic Profiling and Crosstalk with Colorectal Cancer Cells, 5 Cancers (Basel) 15, 350. https://doi.org/10.3390/cancers15020350.

D'Agostino, I., Tacconelli, S., Bruno, A., Contursi, A., Mucci, L., Hu, X., et al., 2021. Low-dose aspirin prevents hypertension and cardiac fibrosis when thromboxane A2 is unrestrained. Pharmacol. Res. 170, 105744. https://doi.org/10.1016/j.phrs.2021.105744.

Dellar, E.R., Hill, C., Melling, G.E., Carter, D.R.F., Baena-Lopez, L.A., 2022. Unpacking extracellular vesicles: RNA cargo loading and function. J. Extracell. Biol. 1, e40. https://doi.org/10.1002/jex2.40.

Deville, S., Garcia Romeu, H., Oeyen, E., Mertens, I., Nelissen, I., Salvati, A., 2022. Macrophages release extracellular vesicles of different properties and composition following exposure to nanoparticles. Int. J. Mol. Sci. 24, 260. https://doi.org/10.3390/ijms24010260.

Domenech, J., Hernández, A., Rubio, L., Marcos, R., Cortés, C., 2020. Interactions of polystyrene nanoplastics with in vitro models of the human intestinal barrier. Arch. Toxicol. 94, 2997–3012. https://doi.org/10.1007/s00204-020-02805-3.

Dovizio, M., Alberti, S., Sacco, A., Guillem-Llobat, P., Schiavone, S., Maier, T.J., et al., 2015. Novel insights into the regulation of cyclooxygenase-2 expression by platelet-cancer cell cross-talk. Biochem. Soc. Trans. 43, 707–714. https://doi.org/10.1042/BST20140322.

Du, Y., Mao, L., Wang, Z., Yan, K., Zhang, L., Zou, J., 2022. Osteopontin – the stirring multifunctional regulatory factor in multisystem aging. Front. Endocrinol. (Lausanne) 13, 1014853. https://doi.org/10.3389/fendo.2022.1014853.

Fan, C., Shi, X., Zhao, K., Wang, L., Shi, K., Liu, Y.J., et al., 2022. Cell migration orchestrates migrasome formation by shaping retraction fibers. J. Cell. Biol. 221, e202109168. https://doi.org/10.1083/jcb.202109168.

Fiegel, J., Ehrhardt, C., Schaefer, U.F., Lehr, C.M., Hanes, J., 2003. Large porous particle impingement on lung epithelial cell monolayers—toward improved particle characterization in the lung. Pharm. Res. 20, 788–796. https://doi.org/10.1023/A:1023441804464.

Gao, N., Rezaee, F., 2022. Airway epithelial cell junctions as targets for pathogens and antimicrobial therapy. Pharmaceutics 14, 2619. https://doi.org/10.3390/pharmaceutics14122619.

García-Rodríguez, A., Gutiérrez, J., Villacorta, A., Arribas Arranz, J., Romero-Andrada, I., Lacoma, A., et al., 2024. Polylactic acid nanoplastics (PLA-NPLs) induce adverse effects on an in vitro model of the human lung epithelium: The Calu-3 air-liquid interface (ALI) barrier. J. Hazard. Mater. 15 475, 134900. https://doi.org/10.1016/j.jhazmat.2024.134900.

Geiser, M., Kreyling, W.G., 2010. Deposition and biokinetics of inhaled nanoparticles. Part. Fibre Toxicol. 7, 2. https://doi.org/10.1186/1743-8977-7-2.

Gigault, J., Halle, A.T., Baudrimont, M., Pascal, P.Y., Gauffre, F., Phi, T.L., et al., 2018. Current opinion: what is a nanoplastic? Environ. Pollut. 235, 1030–1034. https://doi.org/10.1016/j.envpol.2018.01.024.

Giuliani, P., Ballerini, P., Buccella, S., Ciccarelli, R., Rathbone, M.P., Romano, S., et al., 2015. Guanosine protects glial cells against 6-hydroxydopamine toxicity. Adv. Exp. Med. Biol. 837, 23–33. https://doi.org/10.1007/5584_2014_73.

Gou, Z., Wu, H., Li, S., Liu, Z., Zhang, Y., 2024. Airborne micro- and nanoplastics: emerging causes of respiratory diseases. Part. Fibre Toxicol. 21, 50. https://doi.org/10.1186/s12989-024-00613-6.

Grosselink, I.F., Leonhardt, P., Drittij, M.J., Weltjens, E., Jessen, P.J.J., van Belleghem, F. G.A.J., et al., 2026. Potential toxicity of micro- and nanoplastics in primary bronchial epithelial cells of patients with chronic obstructive pulmonary disease. Micro nanoplast 6, 16. https://doi.org/10.1186/s43591-025-00166-1.

He, R.W., Braakhuis, H.M., Vandebriel, R.J., Staal, Y.C.M., Gremmer, E.R., Fokkens, P.H. B., Kemp, C., Vermeulen, J., Westerink, R.H.S., Cassee, F.R., 2021. Optimization of an air-liquid interface in vitro cell co-culture model to estimate the hazard of aerosol exposures. J. Aerosol Sci. 153, 105703. https://doi.org/10.1016/j.jaerosci.2020.105703.

Hellings, P.W., Steelant, B., 2020. Epithelial barriers in allergy and asthma. J. Allergy Clin. Immunol. 145, 1499–1509. https://doi.org/10.1016/j.jaci.2020.04.010.

Ho, C.C., Wu, W.T., Chen, Y.C., Liou, S.H., Yet, S.F., Lee, C.H., Tsai, H.T., Weng, C.Y., Tsai, M.H., Lin, P., 2019. Identification of osteopontin as a biomarker of human exposure to fine particulate matter. Environ. Pollut. 245, 975–985. https://doi.org/10.1016/j.envpol.2018.11.071.

Hsu, W.H., Chen, Y.Z., Chiang, Y.T., Chang, Y.T., Wang, Y.W., Hsu, K.T., et al., 2025. Polystyrene nanoplastics disrupt the intestinal microenvironment by altering bacteria–host interactions through extracellular vesicle-delivered microRNAs. Nat. Commun. 16, 5026. https://doi.org/10.1038/s41467-025-59884-y.

Jenner, L.C., Rotchell, J.M., Bennett, R.T., Cowen, M., Tentzeris, V., Sadofsky, L.R., 2022. Detection of microplastics in human lung tissue using μFTIR spectroscopy. Sci. Total. Environ. 831, 154907. https://doi.org/10.1016/j.scitotenv.2022.154907.

Jiang, W., Liu, Y., Wu, Y., Zhang, L., Zhang, B., Zhou, S., et al., 2024. Polystyrene nanoplastics of different particle sizes regulate the polarization of pro-inflammatory macrophages. Sci. Rep. 14, 16329. https://doi.org/10.1038/s41598-024-67289-y.

Johnson, J.R., Roos, A., Berg, T., Nord, M., Fuxe, J., 2011. Chronic respiratory aeroallergen exposure in mice induces epithelial-mesenchymal transition in the large airways. PLoS. One 6, e16175. https://doi.org/10.1371/journal.pone.0016175.

Kim, N., Park, J.H., Lee, I., Jung, G.S., Lee, J.H., Lee, M.J., et al., 2024. Investigation of cell-to-cell transfer of polystyrene microplastics through extracellular vesicle-mediated communication. Biochem. Biophys. Res. Commun. 734, 150719. https://doi.org/10.1016/j.bbrc.2024.150719.

Kohan, M., Breuer, R., Berkman, N., 2009. Osteopontin induces airway remodeling and lung fibroblast activation in a murine model of asthma. Am. J. Respir. Cell. Mol. Biol. 41, 290–296. https://doi.org/10.1165/rcmb.2008-0307OC.

Kouthouridis, S., Goepp, J., Martini, C., Matthes, E., Hanrahan, J.W., Moraes, C., 2021. Oxygenation as a driving factor in epithelial differentiation at the air–liquid interface. Integr. Biol. (Camb.). 13, 61–72. https://doi.org/10.1093/intbio/zyab002.

Lacroix, G., Koch, W., Ritter, D., Gutleb, A.C., Larsen, S.T., Loret, T., et al., 2018. Air–liquid interface in vitro models for respiratory toxicology research: consensus workshop and recommendations. Appl. Vitr. Toxicol. 4, 91–106. https://doi.org/10.1089/aivt.2017.0034.

Lanuti, P., Guardalupi, F., Corradi, G., Florio, R., Brocco, D., Veschi, S., et al., 2025. CD19.CAR T-cell-derived extracellular vesicles express CAR and kill leukemic cells, contributing to antineoplastic therapy. Blood Adv. 9 (12), 2907–2919. https://doi.org/10.1182/bloodadvances.2024014860.

Latorre, E., Matheus, N., Layunta, E., Alcalde, A.I., Mesonero, J.E., 2014. IL-10 counteracts proinflammatory mediator-evoked oxidative stress in Caco-2 cells. Mediat. Inflamm. 2014, 982639. https://doi.org/10.1155/2014/982639.

Lee, D.F., Lethem, M.I., Lansley, A.B., 2021. A comparison of three mucus-secreting airway cell lines (Calu-3, SPOC1 and UNCN3T) for use as biopharmaceutical models of the nose and lung. Eur. J. Pharm. Biopharm. 167, 159–174. https://doi.org/10.1016/j.ejpb.2021.07.016.

Lee, C.E., Rezaee, F., 2024. Nanoparticles and airway epithelial cells: exploring the impacts and methodologies in toxicity assessment. Int. J. Mol. Sci. 25, 7885. https://doi.org/10.3390/ijms25147885.

Leslie, H.A., van Velzen, M.J.M., Brandsma, S.H., Vethaak, A.D., Garcia-Vallejo, J.J., Lamoree, M.H., 2022. Discovery and quantification of plastic particle pollution in

human blood. Environ. Int. 163, 107199. https://doi.org/10.1016/j.envint.2022.107199.
López-Rodríguez, J.C., González, M., Bogas, G., Mayorga, C., Villalba, M., Batanero, E., 2021a. Epithelial permeability to Ole e 1 is more dependent on the functional state of the bronchial epithelium than on the activity of Der p 1 protease acting as an adjuvant to the bystander allergen. J. Investig. Allergol. Clin. Immunol. 31 (4), 343–346. https://doi.org/10.18176/jiaci.0603.
López-Rodríguez, J.C., Rodríguez-Coira, J., Benedé, S., Barbas, C., Barber, D., Villalba, M. T., et al., 2021b. Comparative metabolomics analysis of bronchial epithelium during barrier establishment after allergen exposure. Clin. Transl. Allergy 11, e12051. https://doi.org/10.1002/clt2.12051.
López-Rodríguez, J.C., Solís-Fernández, G., Barderas, R., Villalba, M., Batanero, E., 2018. Effects of Ole e 1 on human bronchial epithelial cells cultured at the air–liquid interface. J. Investig. Allergol. Clin. Immunol. 28, 186–189. https://doi.org/10.18176/jiaci.0227.
Marchisio, M., Simeone, P., Bologna, G., Ercolino, E., Pierdomenico, L., Pieragostino, D., et al., 2020. Flow cytometry analysis of circulating extracellular vesicle subtypes from fresh peripheral blood samples. Int. J. Mol. Sci. 22, 48. https://doi.org/10.3390/ijms22010048.
Margelidon-Cozzolino, V., Tsicopoulos, A., Chenivesse, C., de Nadai, P., 2022. Role of Th17 Cytokines in Airway Remodeling in Asthma and Therapy Perspectives. Front. Allergy 3, 806391. https://doi.org/10.3389/falgy.2022.806391.
Michelini, S., Mawas, S., Kurešepi, E., Barbero, F., Šimunović, K., Miremont, D., et al., 2025. Pulmonary hazards of nanoplastic particles: a study using polystyrene in in vitro models of the alveolar and bronchial epithelium. J. Nanobiotechnol 23, 388. https://doi.org/10.1186/s12951-025-03419-6.
Michi, A.N., Proud, D., 2021. A toolbox for studying respiratory viral infections using air-liquid interface cultures of human airway epithelial cells. Am. J. Physiol. Lung Cell. Mol. Physiol. 321, L263–L280. https://doi.org/10.1152/ajplung.00141.2021.
Mierzejewski, K., Kurzyńska, A., Golubska, M., Całka, J., Gałęcka, I., Szabelski, M., et al., 2023. New insights into the potential effects of PET microplastics on organisms via extracellular vesicle-mediated communication. Sci. Total. Environ. 904, 166967. https://doi.org/10.1016/j.scitotenv.2023.166967.
Milillo, C., Aruffo, E., Di Carlo, P., Patruno, A., Gatta, M., Bruno, A., et al., 2024. Polystyrene nanoplastics mediate oxidative stress, senescence, and apoptosis in a human alveolar epithelial cell line. Front. Public. Health 12, 1385387. https://doi.org/10.3389/fpubh.2024.1385387.
Paget, V., Dekali, S., Kortulewski, T., Grall, R., Gamez, C., Blazy, K., et al., 2015. Specific Uptake and Genotoxicity Induced by Polystyrene Nanobeads with Distinct Surface Chemistry on Human Lung Epithelial Cells and Macrophages. PLoS. One 10, 1–20. https://doi.org/10.1371/journal.pone.0123297.
Papaporfyriou, A., Loukides, S., Kostikas, K., Simoes, D.C.M., Papatheodorou, G., Konstantellou, E., et al., 2014. Increased levels of osteopontin in sputum supernatant in patients with COPD. Chest 146, 951–958. https://doi.org/10.1378/chest.13-2440.
Pardo, A., Gibson, K., Cisneros, J., Richards, T.J., Yang, Y., Becerril, C., et al., 2005. Up-regulation and profibrotic role of osteopontin in human idiopathic pulmonary fibrosis. PLoS. Med. 2, e251. https://doi.org/10.1371/journal.pmed.0020251.
Pell, Gray, T.J., Hopkins, M.B., Kasprowicz, S.J., Porter, R., Reeves, J.D., et al., 2021. Epithelial barrier integrity profiling: combined approach using cellular junctional complex imaging and transepithelial electrical resistance. SLAS Discov. 26, 909–921. https://doi.org/10.1177/24725552211013077.
Place, T.L., Domann, F.E., Case, A.J., 2017. Limitations of oxygen delivery to cells in culture: an underappreciated problem in basic and translational research. Free. Radic. Biol. Med. 113, 311–322. https://doi.org/10.1016/j.freeradbiomed.2017.10.003.
Plastics – the fast Facts 2024. Plastics Europe. ⟨https://plasticseurope.org/knowledge-hub/plastics-the-fast-facts-2024/⟩ (accessed 9 September 2025).
Rezaee, F., Georas, S.N., 2014. Breaking barriers. New insights into airway epithelial barrier function in health and disease. Am. J. Respir. Cell. Mol. Biol. 50, 857–869. https://doi.org/10.1165/rcmb.2013-0541RT.
Saul, M.J., Baumann, I., Bruno, A., Emmerich, A.C., Wellstein, J., Ottinger, S.M., et al., 2019. miR-574-5p as RNA decoy for CUGBP1 stimulates human lung tumor growth by mPGES-1 induction. FASEB J. 33, 6933–6947. https://doi.org/10.1096/fj.201802547R.
Schlinkert, P., Casals, E., Boyles, M., Tischler, U., Hornig, E., Tran, N., et al., 2015. The oxidative potential of differently charged silver and gold nanoparticles on three human lung epithelial cell types. J. nanobiotechnology 13 (1). https://doi.org/10.1186/s12951-014-0062-4.
Shahzadi, C., Di Serafino, A., Aruffo, E., Mascitelli, A., Di Carlo, P., 2023. A549 as an in vitro model to evaluate the impact of microplastics in the air. Biol. (Basel) 12, 1243. https://doi.org/10.3390/biology12091243.
Sharaf Din, K., Khokhar, M.F., Butt, S.I., Qadir, A., Younas, F., 2024. Exploration of microplastic concentration in indoor and outdoor air samples: morphological, polymeric, and elemental analysis. Sci. Total. Environ. 908, 168398. https://doi.org/10.1016/j.scitotenv.2023.168398.
Shaykhiev, R., Otaki, F., Bonsu, P., Dang, D.T., Teater, M., Strulovici-Barel, Y., et al., 2011. Cigarette smoking reprograms apical junctional complex molecular architecture in the human airway epithelium in vivo. Cell. Mol. Life Sci. 68, 877–892. https://doi.org/10.1007/s00018-010-0500-x.
Siddiqui, S.A., Singh, S., Bahmid, N.A., Shyu, D.J.H., Domínguez, R., Lorenzo, J.M., et al., 2023. Polystyrene microplastic particles in the food chain: characteristics and toxicity. Sci. Total. Environ. 892, 164531. https://doi.org/10.1016/j.scitotenv.2023.164531.
Silva, S., Bicker, J., Falcão, A., Fortuna, A., 2023. Air–liquid interface (ALI) impact on different respiratory cell cultures. Eur. J. Pharm. Biopharm. 184, 62–82. https://doi.org/10.1016/j.ejpb.2023.01.013.
Simeone, P., Celia, C., Bologna, G., Ercolino, E., Pierdomenico, L., Cilurzo, F., et al., 2020. Diameters and fluorescence calibration for extracellular vesicle analyses by flow cytometry. Int. J. Mol. Sci. 21 (21), 7885. https://doi.org/10.3390/ijms21217885.
Singh, A., Chauhan, A., Gaur, R., 2025. A comprehensive review on the synthesis, properties, environmental impacts, and chemiluminescence applications of polystyrene (PS). Discov. Chem. 2, 47. https://doi.org/10.1007/s44371-025-00125-y.
Sousa de Almeida, M., Susnik, E., Drasler, B., Taladriz-Blanco, P., Petri-Fink, A., Rothen-Rutishauser, B., 2021. Understanding nanoparticle endocytosis to improve targeting strategies in nanomedicine. Chem. Soc. Rev. 50, 5397–5434. https://doi.org/10.1039/d0cs01127d.
Srinivasan, B., Kolli, A.R., Esch, M.B., Abaci, H.E., Shuler, M.L., Hickman, J.J., 2015. TEER measurement techniques for in vitro barrier model systems. J. Lab. Autom. 20, 107–126. https://doi.org/10.1177/2211068214561025.
Tang, Q., Tang, K., Markby, G.R., Parys, M., Phadwal, K., MacRae, V.E., et al., 2025. Autophagy regulates cellular senescence by mediating the degradation of CDKN1A/p21 and CDKN2A/p16 through SQSTM1/p62-mediated selective autophagy in myxomatous mitral valve degeneration. Autophagy 21 (7), 1433–1455. https://doi.org/10.1080/15548627.2025.2469315.
Théry, C., Witwer, K.W., Aikawa, E., Alcaraz, M.J., Anderson, J.D., Andriantsitohaina, R., et al., 2018. Minimal information for studies of extracellular vesicles 2018 (MISEV2018): a position statement of the International Society for Extracellular Vesicles and update of the MISEV2014 guidelines. J. Extracell. Vesicles 7, 1535750. https://doi.org/10.1080/20013078.2018.1535750.
Vattanasit, U., Kongpran, J., Ikeda, A., 2023. Airborne microplastics: a narrative review of potential effects on the human respiratory system. Sci. Total. Environ. 904, 166745. https://doi.org/10.1016/j.scitotenv.2023.166745.
Viana, M., Tonin, F.S., Ladeira, C., 2025. Assessing the impact of nanoplastics in biological systems: systematic review of in vitro animal studies. J. Xenobiot. 15, 75. https://doi.org/10.3390/jox15030075.
Vouitsis, I., Portugal, J., Kontses, A., Karlsson, H.L., Faria, M., Elihn, K., et al., 2023. Transport-related airborne nanoparticles: Sources, different aerosol modes, and their toxicity. Atmos. Environ. 301, 119698. https://doi.org/10.1016/j.atmosenv.2023.119698.
Wang, Y.L., Huang, C.C., Zheng, C.M., Liu, W.C., Lee, Y.H., Chiu, H.W., 2024. Polystyrene microplastic-induced extracellular vesicles cause kidney-related effects in the crosstalk between tubular cells and fibroblasts. Ecotoxicol. Environ. Saf. 273, 116098. https://doi.org/10.1016/j.ecoenv.2024.116098.
Welsh, J.A., Goberdhan, D.C.I., O'Driscoll, L., Buzas, E.I., Blenkiron, C., Bussolati, B., et al., 2024. Minimal information for studies of extracellular vesicles (MISEV2023): from basic to advanced approaches. J. Extracell. Vesicles 13, e12404. https://doi.org/10.1002/jev2.12404.
Welsh, J.A., van der Pol, E., Arkesteijn, G.J.A., Bremer, M., Brisson, A., Coumans, F., et al., 2020. MIFlowCyt-EV: a framework for standardized reporting of extracellular vesicle flow cytometry experiments. J. Extracell. Vesicles 9, 1713526. https://doi.org/10.1080/20013078.2020.1713526.
Wright, S., Cassee, F.R., Erdely, A., Campen, M.J., 2024. Micro- and nanoplastics concepts for particle and fibre toxicologists. Part. Fibre Toxicol. 21, 18. https://doi.org/10.1186/s12989-024-00581-x.
Wu, Q., Liu, C., Liu, D., Wang, Y., Qi, H., Liu, X., et al., 2024. Polystyrene nanoplastics-induced lung apoptosis and ferroptosis via ROS-dependent endoplasmic reticulum stress. Sci. Total. Environ. 912, 169260. https://doi.org/10.1016/j.scitotenv.2023.169260.
Xie, Y., Li, Y., Feng, Y., Cheng, W., Wang, Y., 2022. Inhalable microplastics prevail in air: exploring the size detection limit. Environ. Int. 162, 107151. https://doi.org/10.1016/j.envint.2022.107151.
Xu, H., Lou, W., Fu, F., 2019. Association between osteopontin expression and asthma: a meta-analysis. J. Int. Med. Res. 47, 3513–3521. https://doi.org/10.1177/0300060519860684.
Zhai, Z., Liu, B., Yu, L., 2023. The roles of migrasome in development. Cell Insight 3 (1), 100142. https://doi.org/10.1016/j.cellin.2023.100142. Nov 28.
Zhang, N., Li, P., Lin, H., Shuo, T., Ping, F., Su, L., et al., 2021. IL-10 ameliorates PM2.5-induced lung injury by activating the AMPK/SIRT1/PGC-1α pathway. Environ. Toxicol. Pharmacol. 86, 103659. https://doi.org/10.1016/j.etap.2021.103659.